LCC-0080
CBP Tech Note-244
May 2002

Linear Collider Collaboration Tech Notes

Estimates of Collective Effects in the NLC Main Damping Rings

A. Wolski and S. de Santis

Lawrence Berkeley National Laboratory
Berkeley, California

Abstract: Damping Ring performance depends on the ability to store the design beam current, and extract the beam with the specified low transverse emittance. Given the high bunch charge and moderate energy, a variety of collective effects could play a significant role, in either limiting the bunch current, or increasing the emittance. Here, we estimate the consequences of various effects, based on current theories and understanding.

LCC-0080
CBP Tech Note-244

Estimates of Collective Effects in the NLC Main Damping Rings

A. Wolski and S. de Santis
Lawrence Berkeley National Laboratory

May 1st, 2002

Abstract

Damping Ring performance depends on the ability to store the design beam current, and extract the beam with the specified low transverse emittance. Given the high bunch charge and moderate energy, a variety of collective effects could play a significant role, in either limiting the bunch current, or increasing the emittance. Here, we estimate the consequences of various effects, based on current theories and understanding.

1 Introduction

Collective effects that have the potential to disrupt beam quality or stability in the NLC Main Damping Rings include:

- long-range (i.e. bunch-to-bunch) wake fields, from RF cavity higher order modes or the resistance of the vacuum chamber walls;
- short-range (i.e. single bunch) wake fields, from components such as BPMs, bellows masks etc.
- intra-beam scattering;
- long and short-range wake fields from electron cloud (positron ring);
- wake fields from ions (electron ring);
- the space-charge impedance of the bunch itself.

Some of these effects, such as the wake fields from vacuum chamber components, are relatively well understood, although difficult to predict with confidence in particular situations. In other cases, notably for the intra-beam scattering and electron cloud, the theory is less well developed, and the experimental data surrounded by significant uncertainty. Since many of the effects are related (e.g. by affecting and being affected by the bunch volume), we review here the impact each is likely to have on operation of the MDRs.

Some parameters for the present MDR design[1] are given in Table 1.

Table 1

NLC MDR parameters.

Energy	E	1.98 GeV
Circumference	C	299.792 m
Tunes	ν_x, ν_y, ν_s	27.26, 11.14, 0.0035
Mean beta functions	$\langle\beta_x\rangle$, $\langle\beta_y\rangle$	3.6 m, 7.1 m
Momentum compaction	α	2.95×10^{-4}
Natural energy spread	σ_δ	0.0909 %
Bunch length	σ_z	3.60 mm
RF acceptance (at 1.07 MV)		1.5 %
Particles per bunch	N_b	7.5×10^{9}
Bunch separation	s_b/c	1.4 ns
Fill pattern		3 trains of 192 bunches
RF frequency	f_{RF}	714 MHz
Energy loss per turn	U_0	792 keV
Radiation damping times	τ_x, τ_y, τ_ε	4.76 ms, 5.00 ms, 2.57 ms
Equilibrium normalized emittance	$\gamma\varepsilon_x$, $\gamma\varepsilon_y$	2.22 μm, 0.0131 μm
Mean horizontal $\mathcal{H}$ function	$\langle\mathcal{H}_x\rangle$	1.91 mm
Vacuum chamber material		Aluminum
Beam pipe radius: standard, wiggler	b	0.016 mm, 0.008 mm

2 Coupled-Bunch Instabilities

Long-range wake fields driving coupled-bunch instabilities arise from RF cavity and vacuum chamber impedances, and also from electron cloud (positron ring) or ions (electron ring). In this section, we consider the impedance sources; electron cloud and ion effects are discussed in sections 8 and 9 respectively.

For an arbitrary fill function, calculation of the longitudinal and transverse coupled-bunch growth rates can be extremely cumbersome, since modulation coupling and Landau damping have to be taken into account. In our case, where we are dealing with three trains of equally charged, uniformly separated bunches, we can derive useful information about the upper boundaries of the growth rates, by studying uniform fills[2].

2.1 Longitudinal growth rates

Given a uniform fill, the growth rate for the *p*-th longitudinal coupled-bunch mode is:

$$\frac{1}{\tau} = \frac{I_0 \alpha f_{RF}}{2E\nu_s} \mathrm{Re}\left[Z_{//}^{eff}(p)\right]$$

where I_0 is the total current. The effective impedance $Z_{//}^{eff}(p)$ for the *p*-th mode is the sum of all the longitudinal modes of the RF cavities at the modal harmonics $f_p(n)$:

$$f_p(n) = nf_{RF} + (p + \nu_s) f_0$$

$$Z_{//}^{eff}(p) = \sum_{n=-\infty}^{\infty} Z_{//}(f_p) \frac{|f_p|}{f_{RF}} \exp\left[-\left(2\pi \frac{f_p \sigma_z}{c} \right)^2 \right]$$

f_0 is the revolution frequency. The longitudinal growth rates for the MDRs are shown in Figure 1. The black dots are obtained by analyzing a uniform fill with the same current per bunch as the actual three-train fill, and thus with a higher current. In the case of a single gap in the fill, it can be demonstrated analytically[3] that these are indeed the upper limits of the growth rates. The additional two gaps present in the MDR cause an additional coupling between modes whose indices differ by three. An analysis of the power spectrum of the three-train fill shows that this is only a small effect. The filled areas are obtained from an analysis of a uniform fill with the same total current, and therefore less current per bunch, as the actual fill. This gives an estimate of the lower limit for the growth rates, even though modulation coupling can couple stable modes to unstable ones, resulting in a lower growth rate for some modes. The only mode above threshold is caused by the accelerating mode detuning (~114 kHz).

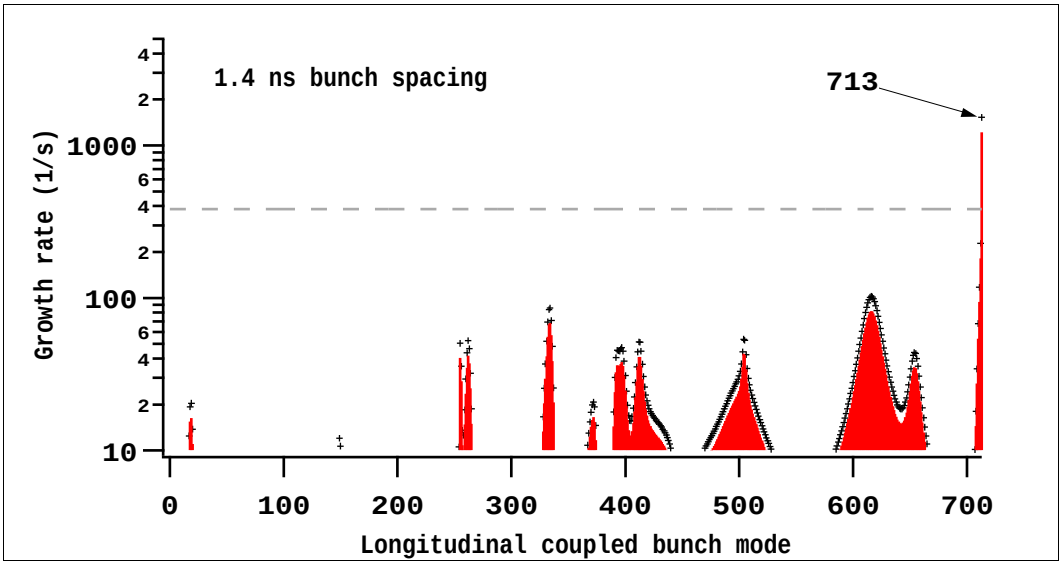

Figure 1

Longitudinal growth rates in the MDRs. The dashed line shows the radiation damping.

2.2 Transverse growth rates

At present, there are no separate data available for horizontal and vertical transverse higher-order modes (which would require full 3-D simulations of the RF cavities[4], if not measurements on a prototype), so the only difference between horizontal and vertical growth rates arises from the difference in the betatron tunes.

The transverse growth rates for a uniform fill are:

$$\frac{1}{\tau} = \frac{I_0 f_{RF} \beta_{x,y}}{2E} \mathrm{Re}\left[Z_{\perp}^{eff}(p)\right]$$

The modal harmonics at which the effective transverse impedance is to be evaluated are given by:

$$f_p(n) = n f_{RF} + \left(p + \nu_{x,y}\right) f_0$$

and the effective transverse impedance for the *p*-th mode is:

$$Z_{\perp}^{eff}(p) = -\sum_{n=-\infty}^{\infty} \left(Z_{\perp,HOM}(f_p) + Z_{\perp,RW}(f_p)\right) \mathrm{sgn}(f_p) \exp\left[-\left(2\pi \frac{f_p \sigma_z}{c}\right)^2\right]$$

In this case, positive frequency harmonics are damping. The resistive wall transverse impedance for an aluminum vacuum chamber is given by:

$$Z_{\perp,RW}(f) = (1-\mathrm{i}) 0.81 \sqrt{\frac{f_0}{f}} \ \mathrm{M\Omega/m}$$

We can calculate upper and lower limits for the growth rates for the three-train fill, using the same method as in the longitudinal case.

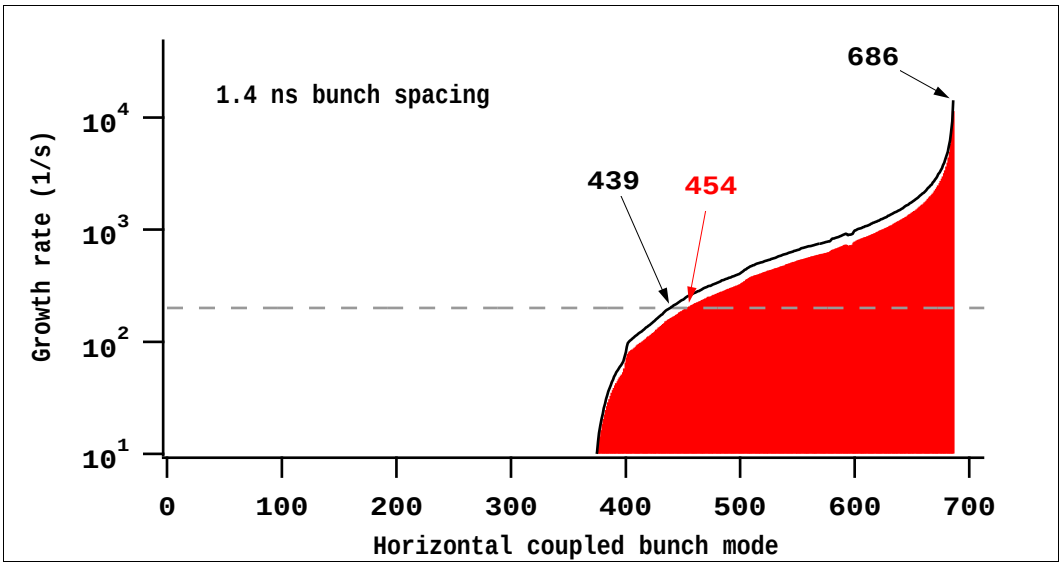

Figure 2a

Horizontal coupled-bunch growth rates in the MDRs, including resistive wall impedance. The dashed line gives the radiation damping.

The resistive wall impedance dominates the growth rates, and there would be little advantage of developing the cavity design to damp further the higher order modes. The range of modes with growth rates faster than the radiation damping rate indicates that a feedback system will be required, with bandwidth of the order 350 MHz, and sufficient gain to damp modes with growth times of the order 100 μs.

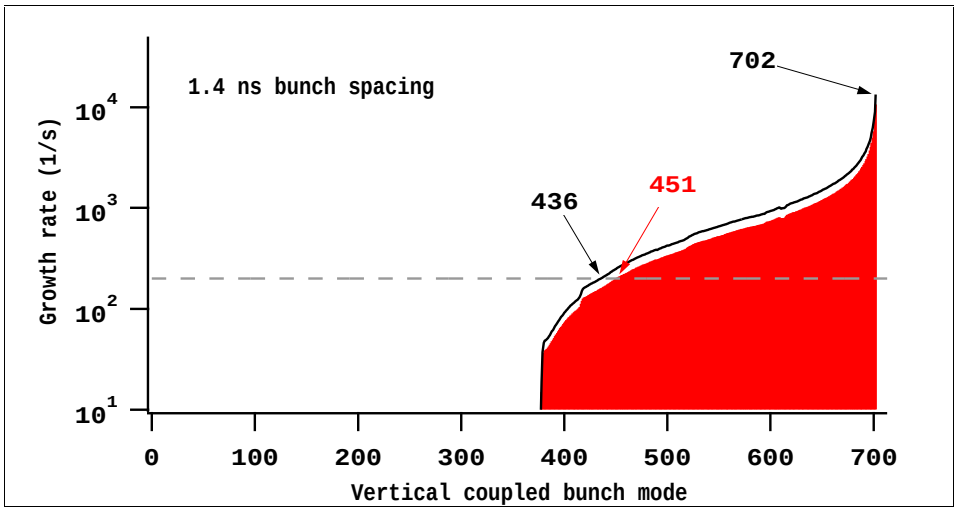

Figure 2b

Vertical coupled-bunch growth rates in the MDRs, including resistive wall impedance. The dashed line gives the radiation damping.

3 Short-Range Wake Fields

An impedance model for an earlier version of the MDR was developed by Ng[5]. It appears that the present design, in terms of circumference, vacuum chamber dimensions, numbers of BPMs and other components, resembles this previous version sufficiently closely for the model to retain some validity. In particular, the large contribution from the resistive wall may be compared with the wake field calculated analytically, and is found to match closely. The total wake potential, including contributions from the RF cavities, resistive wall, BPMs, bellows masks, antechamber slots, and injection/extraction kickers, is shown in Figure 3.

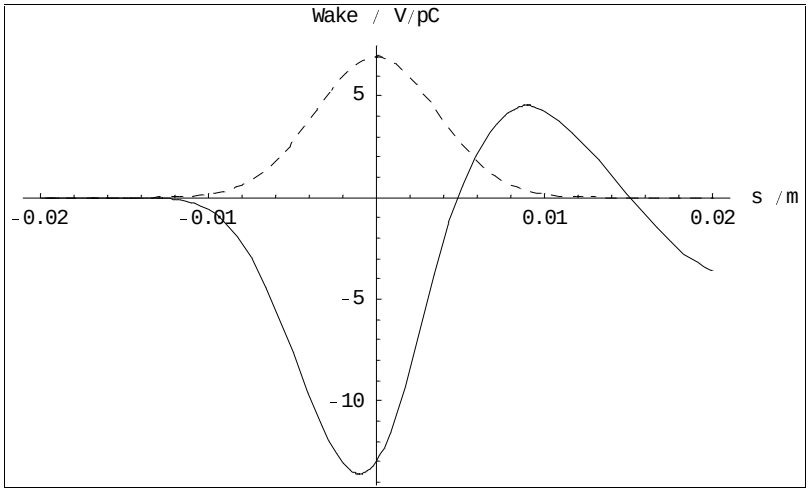

Figure 3

Short range wake potential, drawn from reference 5. The broken line shows the bunch shape used to generate the wake potential in the MAFIA simulation.

We consider here two consequences of the short-range wake field; potential well distortion, and the microwave instability threshold.

3.1 Potential well distortion

The short-range wake field leads to a modification of the longitudinally focusing potential seen by particles in the beam; this is essentially a stationary mode driven by the broad band impedance of the ring. The equilibrium longitudinal distribution of particles in the bunch may be found by solving the Haissinski equation:

$$\rho(z) = \rho(0)\exp\left[-\frac{1}{2}\left(\frac{\omega_s z}{\alpha c \sigma_\delta}\right)^2 + \frac{r_e}{\alpha\sigma_\delta^2\gamma C}\int_0^z dz''\int_{z''}^{\infty} dz'\rho(z')W_0'(z''-z')\right]$$

$$\int_{-\infty}^{\infty}\rho(z)dz = N_b$$

where ρ is the line density of charge in the bunch, ω_s the synchrotron frequency, γ the relativistic factor, and W_0' the longitudinal wake function (other parameters are defined in Table 1). The wake potential is generated numerically by modeling in MAFIA, using a bunch of non-zero length; the potential found in this way has a leading tail that is not physical. This may be dealt with in either of two ways: by replacing the tail with a delta function of the same area at $z = 0$ (the resistive approximation), or by reflecting the leading tail in the plane $z = 0$ (the capacitative approximation). If a sufficiently short bunch has been used to generate the wake potential, both approximations should give the same result. The solution to the Haissinski equation for the wake potential of Figure 3 is shown in Figure 4.

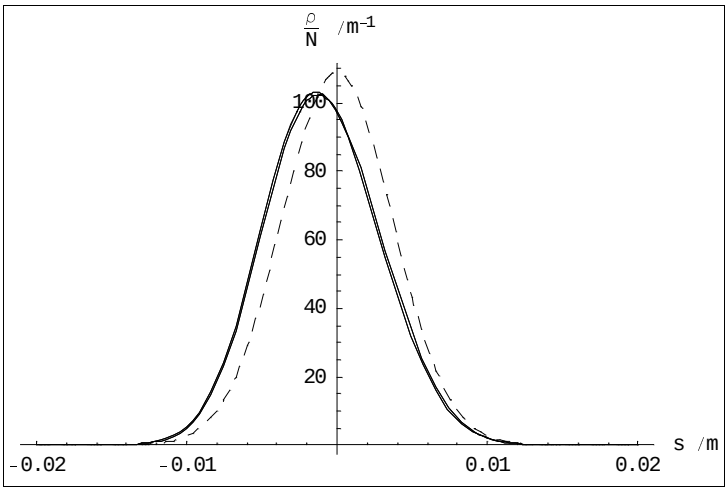

Figure 4

Effect of potential well distortion on the longitudinal bunch distribution. The broken line shows the zero-current limit; the two solid lines show the bunch distribution using the resistive and capacitative approximations.

The bunch length is increased by approximately 4.5% as a result of the broad-band impedance. This is unlikely to have any significant effect on other collective effects,

such as intra-beam scattering or Touschek lifetime. The energy loss resulting from the trapped modes is roughly 10 keV, and the synchronous phase is shifted by a corresponding amount.

3.2 Microwave instability threshold

It is possible to obtain an estimate of the microwave instability threshold using the Boussard criterion. One considers beam oscillations driven by the broad-band impedance; the allowed frequencies of oscillation must satisfy a condition, expressed as a dispersion relation, arising from Landau damping. The Boussard criterion gives an approximation to the region of stability in the complex plane representing the impedance:

$$\frac{|Z_{//}|}{n} \leq \frac{2\pi\alpha E\sigma_\delta^2}{e\hat{I}}$$

where $Z_{//}(\omega)$ is the longitudinal impedance, E is the beam energy, and $\hat{I}$ is the peak current. From the bunch shape and wake potential shown in Figure 3, we can fit an impedance to the induced voltage; the result is shown in Figure 5.

The magnitude of the impedance is 327 Ω. We use c/σ_z for the characteristic frequency, so that $n = c/\omega_0\sigma_z$, and $|Z_{//}|/n \approx 0.025\Omega$. The Boussard criterion then gives for the microwave threshold:

$$\hat{I} \leq 120\,\mathrm{A}$$

Since the nominal peak current is 40 A, there appears to be a margin of a factor of three between the operating point and the threshold.

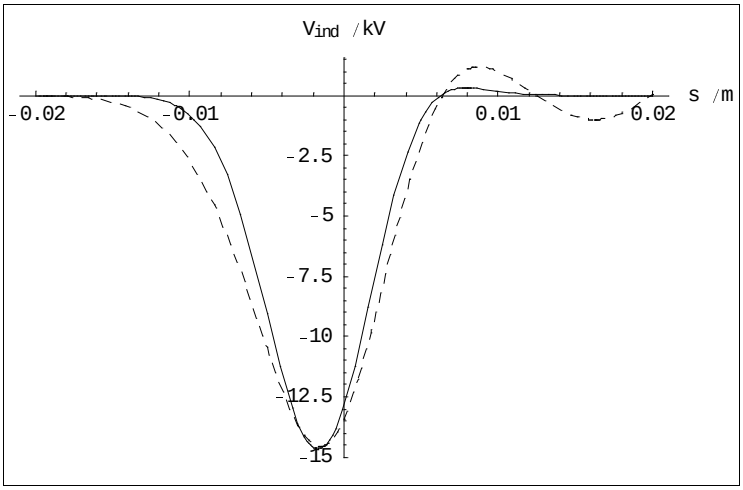

Figure 5

The broken line shows the induced voltage from the bunch shape and wake potential of Figure 3. The broken line shows a fit to this induced voltage, using a resistive impedance of 327 Ω, with a small inductive component.

The Boussard criterion gives a somewhat rough estimate of the microwave threshold. A more rigorous approach involves solving the linearized Vlasov equation, to find the

longitudinal modes. It is also possible to estimate the threshold through turn-by-turn tracking, using a large number of macroparticles. Estimates for the damping ring design used in the NLC ZDR[6] found qualitative agreement between the different approaches, with the Boussard criterion possibly giving an optimistic estimate of the operating margin.

4 Touschek Lifetime

Touschek scattering is the dominant lifetime limitation in low emittance electron storage rings. Collisions between particles in a given bunch lead to a transfer of transverse momentum to the longitudinal. Since the transverse momentum of a particle is typically very much larger than longitudinal (in the rest frame of the bunch), such collisions can lead to particles being scattered outside the momentum acceptance of the ring, defined either by the RF voltage, transverse dynamics, or physical aperture. The rate at which particles are lost clearly depends on the collision rate, and hence on the bunch volume, and on the momentum acceptance. Third generation light sources typically increase the bunch volume by transverse emittance coupling or higher harmonic cavities, to achieve Touschek lifetimes of several hours. The aim in a damping ring is to reduce the bunch volume (certainly in the transverse dimensions) as much as possible. Given the moderate energy of the beam in the NLC MDR, the Touschek lifetime may be expected to be of the order of minutes rather than hours. Since in standard operation, each bunch is stored for only a few milliseconds, Touschek scattering is unlikely to be an operational limitation; however, a reasonable lifetime is desirable for commissioning and regular tuning of the ring.

We can estimate the Touschek lifetime in the MDR using the standard formula[7]:

$$\frac{1}{\tau} = -\frac{1}{N_b}\frac{\mathrm{d}N_b}{\mathrm{d}t} = \frac{r_e^2 c N_b \lambda^3 D(\varepsilon)}{8\pi\gamma^2\sigma_x\sigma_y\sigma_z}$$

where $\lambda^{-1} = \Delta p_{\max} / p_0$ is given by the momentum acceptance, and σ_x, σ_y, σ_z are respectively the rms bunch width, height and length. The function $D(\varepsilon)$ is defined by:

$$D(\varepsilon) = \sqrt{\varepsilon}\left[-\tfrac{3}{2}\mathrm{e}^{-\varepsilon} + \frac{\varepsilon}{2}\int_\varepsilon^\infty \frac{\ln u}{u}\mathrm{e}^{-u}\mathrm{d}u + \tfrac{1}{2}(3\varepsilon - \varepsilon\ln\varepsilon + 2)\int_\varepsilon^\infty \frac{\mathrm{e}^{-u}}{u}\mathrm{d}u\right]$$

and the parameter ε is given by $\varepsilon^{-1} = (\gamma\lambda\sigma_x')^2$, with σ_x' the horizontal beam divergence. The results of the calculation are shown in Figure 6, where we see the lifetime of the beam increasing as roughly the third power of the momentum acceptance ($D(\varepsilon)$ is a rather flat function of the momentum acceptance in this regime). The RF power is specified to give a momentum acceptance of 1.5%, which would imply a lifetime of around 4 minutes. The dynamic momentum acceptance of the lattice may be somewhat less than this, although further optimization of the dynamics could improve the situation. We note that the lifetime scales as the square root of the vertical emittance, and is inversely proportional to the bunch charge. Increasing the emittance ratio to about 5% would give a lifetime of the order 10 minutes.

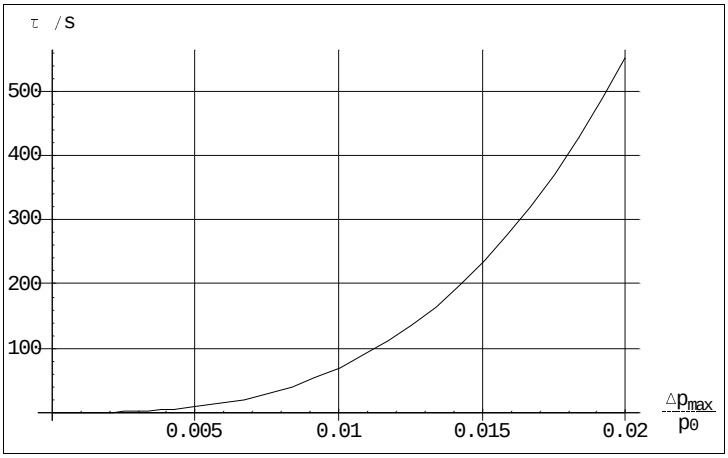

Figure 6

Touschek lifetime in the MDR as a function of momentum acceptance of the ring, with the nominal 0.013 μm rad normalized vertical emittance.

The beam loss from Touschek scattering will lead to some radiation load on the ring. However, with a lifetime of 200 s, the expected power load from this source is less than 10 W, which should not be a significant problem.

5 Intra-beam Scattering

Collisions between particles in a bunch may lead to a small enough transfer of momentum, that the particles involved are not lost from the beam. In this case, there is an increase in the energy spread of the bunch, which couples back through the dispersion into the transverse planes. The resulting emittance increase may be estimated using one of the theories of intra-beam scattering (IBS). Here, we apply formulae[8] giving approximations to the more rigorous treatment of Bjorken and Mtingwa[9]; the results of the different approaches are generally in reasonable agreement[10]. The IBS growth rates are defined as:

$$\frac{1}{T_\delta}=\frac{1}{\sigma_\delta}\frac{\mathrm{d}\sigma_\delta}{\mathrm{d}t} \qquad \frac{1}{T_x}=\frac{1}{\sqrt{\varepsilon_x}}\frac{\mathrm{d}\sqrt{\varepsilon_x}}{\mathrm{d}t} \qquad \frac{1}{T_y}=\frac{1}{\sqrt{\varepsilon_y}}\frac{\mathrm{d}\sqrt{\varepsilon_y}}{\mathrm{d}t}$$

and are given by:

$$\begin{aligned}\frac{1}{T_\delta} &\approx \frac{r_e^2 c N_b}{32\gamma^3\varepsilon_x\varepsilon_y\sigma_z\sigma_\delta^2}\sqrt[4]{\frac{\varepsilon_x\varepsilon_y}{\langle\beta_x\rangle\langle\beta_y\rangle}}\ln\left(\frac{\langle\sigma_y\rangle\gamma^2\varepsilon_x}{r_0\langle\beta_x\rangle}\right)\\ \frac{1}{T_{x,y}} &\approx \frac{\sigma_\delta^2\langle\mathcal{H}_{x,y}\rangle}{\varepsilon_{x,y}}\frac{1}{T_\delta}\end{aligned} \qquad (1)$$

where the lattice function $\mathcal{H}_x$ is defined in terms of the dispersion:

$$\mathcal{H}_x=\gamma_x\eta_x^2+2\alpha_x\eta_x\eta_x'+\beta_x\eta_x^2$$

and similarly for the vertical plane. Brackets $\langle\ \rangle$ indicate averages over the full lattice.

Assuming that the vertical dispersion is randomly distributed around the ring, then the vertical emittance generated by the vertical dispersion may be approximated by:

$$\varepsilon_y \approx 2J_\varepsilon \left\langle \mathcal{H}_y \right\rangle \sigma_\delta^2 \tag{2}$$

where J_ε is the longitudinal damping partition number.

There exists an analogy between emittance growth from IBS and emittance growth from quantum radiation. In both cases, change in the momentum deviation of a particle in a dispersive region of the lattice results in a change in betatron oscillation amplitude. The growth rate of the emittance in either process follows from a consideration of the statistics of the transverse excitation. The difference between the two processes, is that IBS occurs throughout the lattice, whereas quantum excitation takes place only where synchrotron radiation is emitted, i.e. in magnetic fields. There follows a relationship between the relative IBS emittance growth in the vertical and horizontal planes, which may be expressed as:

$$\frac{I_5}{I_3 \left\langle \mathcal{H}_x \right\rangle} \le \frac{\Delta\varepsilon_y / \varepsilon_y}{\Delta\varepsilon_x / \varepsilon_x} \le 1 \tag{3}$$

where I_3 and I_5 are the third and fifth synchrotron radiation integrals. The range on the relative IBS emittance growth is a consequence of the different mechanisms by which vertical emittance may be generated: in the case the vertical emittance is dominated by betatron coupling, the relative growth will be close to 1; in the case it is dominated by vertical dispersion, it will be close to the limit given by the radiation integrals and the average of $\mathcal{H}_x$. The low vertical dispersion limit may easily be understood by inspection of equations (2) and (3). If the vertical dispersion throughout the lattice is zero then $\left\langle \mathcal{H}_y \right\rangle = 0$, and the vertical emittance and IBS vertical growth rate are both expected to be zero. Any vertical emittance comes from betatron coupling from the horizontal plane, and the relative vertical emittance growth from IBS must then equal the relative horizontal emittance growth.

For a lattice where all bends are the same strength equation (3) reduces to[11]:

$$\frac{\left\langle \mathcal{H}_x \right\rangle_{bends}}{\left\langle \mathcal{H}_x \right\rangle} \le \frac{\Delta\varepsilon_y / \varepsilon_y}{\Delta\varepsilon_x / \varepsilon_x} \le 1 \tag{4}$$

For the NLC MDR, this is a poor approximation, since the wiggler makes a dominant contribution to the radiation energy loss.

Solutions to equations (1) for the case of 0.1% betatron coupling are shown in Figure 7. We note that the horizontal emittance passes through a minimum before rising to an equilibrium value; this is characteristic of IBS, and has been observed at the ATF[12]. The behavior is easily explained, since the scattering rate depends on the bunch volume, and the horizontal IBS emittance growth only becomes significant once the vertical emittance has damped below a certain value.

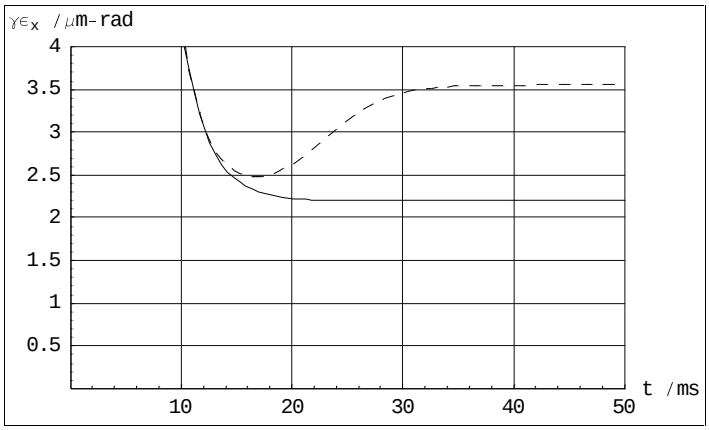

(a) Horizontal emittance

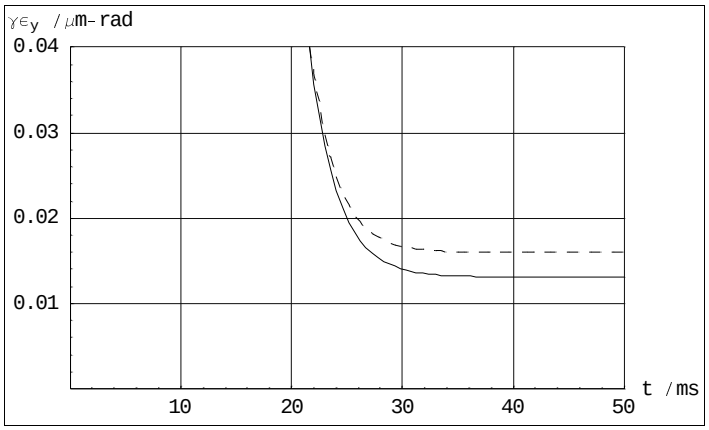

(b) Vertical emittance

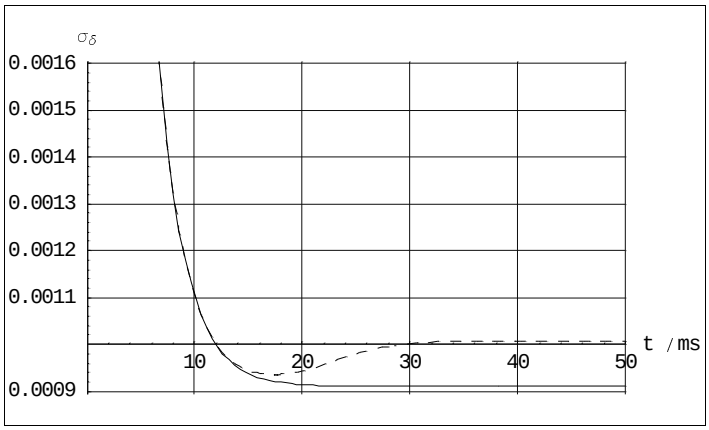

(c) Energy spread

Figure 7

Damping without IBS (solid lines) and with IBS (broken lines), in (a) the horizontal (b) the vertical planes, and (c) the energy spread. The initial horizontal and vertical emittances are 150 μm-rad, and the initial energy spread is 1%. The beam is extracted after 25 ms. For the IBS calculations, a betatron coupling of 0.1% was assumed, with an equilibrium vertical emittance of 0.013 μm-rad.

The results of some calculations are shown in Table 2. We note that for the MDR lattice, $I_5 / I_3 \langle \mathcal{H}_x \rangle \approx 0.2$; the relative emittance growth is then consistent with the condition given in equation (4).

IBS theory has not been rigorously tested in the regime in which the MDR is designed to operate, although studies are continuing at the ATF and the ALS[13]. Some of the results from the ATF suggest that the Coulomb log factor (the logarithm of the ratio of maximum to minimum impact parameters in the collision between any two particles in the bunch) may be as much as a factor of two larger than expected. The IBS growth rates are directly proportional to the Coulomb log (see the logarithmic factor in equation (1)), so uncertainty in this factor has a large impact on the size of the predicted effect. Even with the conventional theory, the extracted emittances have values larger than the specifications; we suggest that research in this area should be continued.

Table 2

Effects of IBS on horizontal and vertical emittance.

Time	Betatron Coupling	No IBS		With IBS		Relative Emittance Growth
		$\gamma\varepsilon_x$/μm	$\gamma\varepsilon_y$/μm	$\gamma\varepsilon_x$/μm	$\gamma\varepsilon_y$/μm	
Equilibrium	0	2.20	0.0131	3.62	0.0147	0.2
Equilibrium	0.001	2.20	0.0131	3.55	0.0160	0.4
Equilibrium	0.006	2.20	0.0131	3.37	0.0206	1.0
Extraction	0.001	2.20	0.0200	3.14	0.0219	-

To compensate for the effects of IBS, several approaches are possible. The IBS growth rates decrease with increasing energy; however, increasing the energy with the present lattice design leads to an increase in the extracted emittance, because of the increase in the natural emittance of the lattice. A new lattice would therefore be needed to benefit from an energy increase. An alternative approach might be to use higher harmonic cavities to increase the bunch length, thus reducing the scattering rate by increasing the bunch volume. The results of some calculations of extracted emittance as a function of bunch length, are shown in Figure 8. It appears that a bunch lengthening of the order of 40%, together with some modest reduction in the equilibrium vertical emittance, would be sufficient to reduce the extracted emittances to within the specified limits.

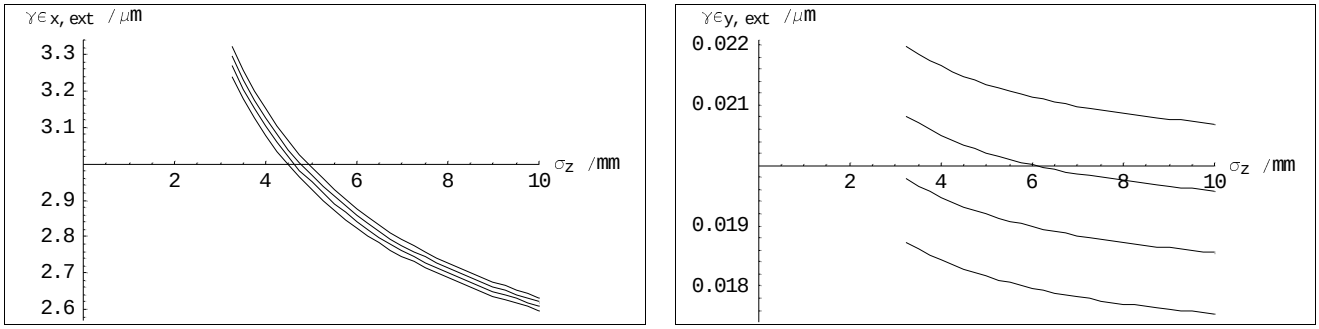

(a) Horizontal emittance **(b) Vertical emittance**

Figure 8

Extracted emittance as a function of bunch length, with IBS, using the conventional value for the Coulomb log. The different lines correspond to equilibrium vertical emittances between 0.010 μm rad (upper line for the horizontal plot, and lower line for the vertical) and 0.013 μm rad.

The main problem with using higher harmonic cavities is that the beam loading leads to phase transients in the bunch trains, that can be strongly nonlinear; the likely effects of harmonic cavities in the MDR are currently being investigated. We present some initial results in the next section.

The variation of the horizontal emittance during the damping cycle shown in Figure 7 raises the possibility of overcoming the limitation from IBS by *lowering* the energy by a small amount. The idea is to increase the damping time, so that extraction takes place closer to the minimum of the horizontal emittance. We rely on there being some margin

between the equilibrium horizontal emittance without IBS (2.2 μm rad), and the specified extracted emittance (3.0 μm rad). The drawback to this approach, is of course that there has to be a significant reduction in the equilibrium vertical emittance to compensate the lower damping rate.

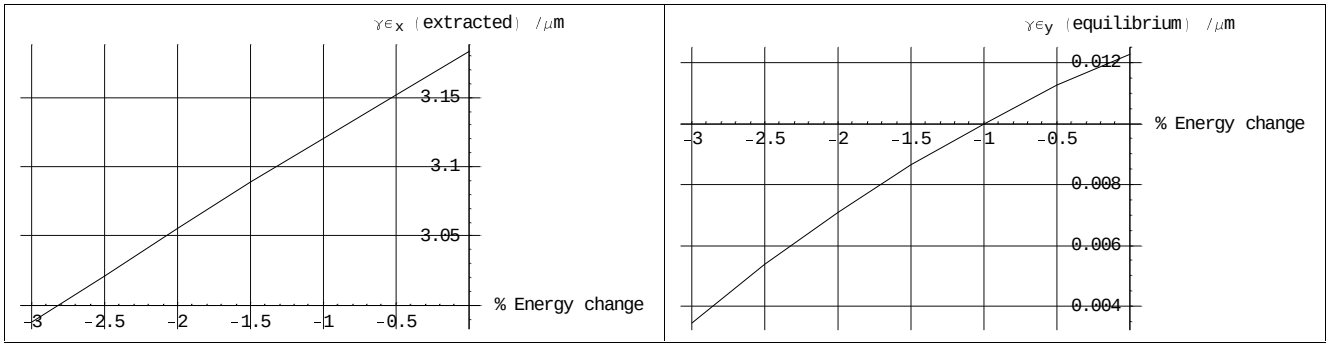

Figure 9

Horizontal extracted emittance and required (zero current) equilibrium vertical emittance, as functions of change in the beam energy. The extracted vertical emittance is fixed at 0.02 μm rad.

In Figure 9, we show the extracted horizontal emittance as a function of the change in energy, and the equilibrium vertical emittance required to allow 0.02 μm rad extracted vertical emittance. A reduction in energy by about 3% will produce the specified extracted horizontal emittance, but the equilibrium vertical emittance needs to be reduced by a factor of 3. There would clearly be a significant impact on the alignment tolerances, but we have not yet investigated this.

6 Phase Transients from Beam Loading

Gaps between the bunch trains in a storage ring lead to a variation in the synchronous phase along the bunch trains. This effect has been studied using a tracking code based on difference equations used to model the longitudinal motion of each individual bunch[14]:

$$\delta_{n+1} = \left(1 - \frac{2T_0}{\tau_\varepsilon}\right)\delta_n + \frac{e}{E}\left(V_g(\phi_n) + V_b(\phi_n)\right) - \frac{U_0}{E}$$

$$\phi_{n+1} = \phi_n + 2\pi\alpha h\delta_{n+1}$$

where δ is the momentum deviation, ϕ the beam phase with respect to the synchronous phase, T_0 is the revolution period, V_g the generator voltage, V_b the beam induced voltage, and h the harmonic number. For these simulations, we assumed that there was no limitation in the available RF power (i.e. the compensation for beam loading was unlimited).

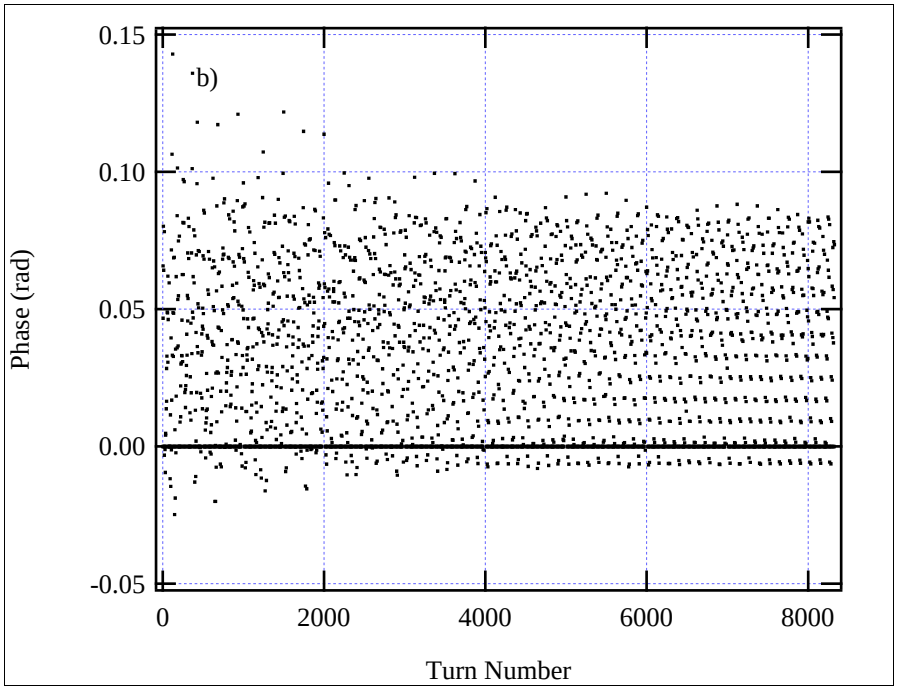

Figure 10

Longitudinal phase of a subset of bunches, tracked over one injection/extraction cycle.

Figure 6 shows the evolution in longitudinal phase of a small number of bunches, tracked over a number of turns corresponding to a single injection/extraction cycle. The initial phase and energy deviation are chosen randomly. Because of the radiation damping, the equilibrium is reached after about 5000 turns; this is shown in Figure 11. The equilibrium peak-to-peak phase variation is slightly less than 100 mrad, which corresponds to 6.8 mm in the ring.

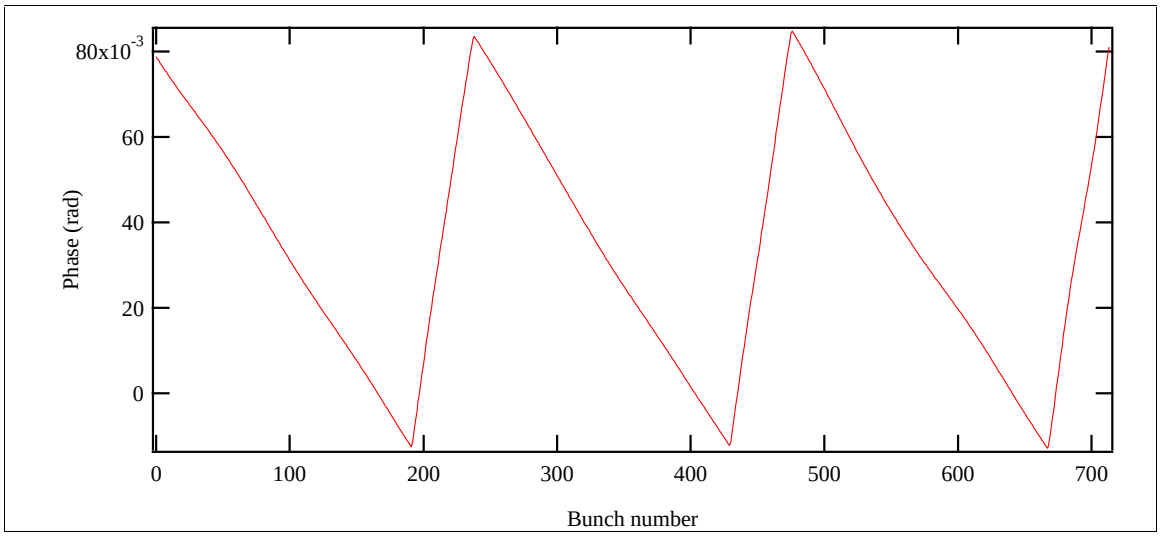

Figure 11

Equilibrium distribution of phases along an MDR fill. The positive slopes occur at the gaps, represented in the simulation by bunches with zero charge.

As a further test, starting from the equilibrium distribution, the phases and energy deviations in a single train were randomized, to simulate the injection of a new train. The behavior of the new and older trains does not differ significantly from that shown in Figure 10 and Figure 11, except over the first few hundred turns. Further work is underway to calculate the influence of higher order modes in the RF cavities, of saturation in the RF generator, and of unequal bunch charges within a train.

7 Space-Charge

Focusing effects from the space-charge force of the bunch leads to an incoherent tune shift, which may not be entirely negligible for highly focused beams at moderate energy. Using the standard formula[7]:

$$\Delta\nu_y = \frac{r_e N_b}{(2\pi)^{3/2}\sigma_z\gamma^3}\oint\frac{\beta_y}{\sigma_y(\sigma_x+\sigma_y)}\mathrm{ds}$$

we find that the incoherent vertical tune shift is 0.05 for the equilibrium beam, and 0.04 for the beam at extraction. The horizontal tune shift is much smaller, because of the larger horizontal size of the beam.

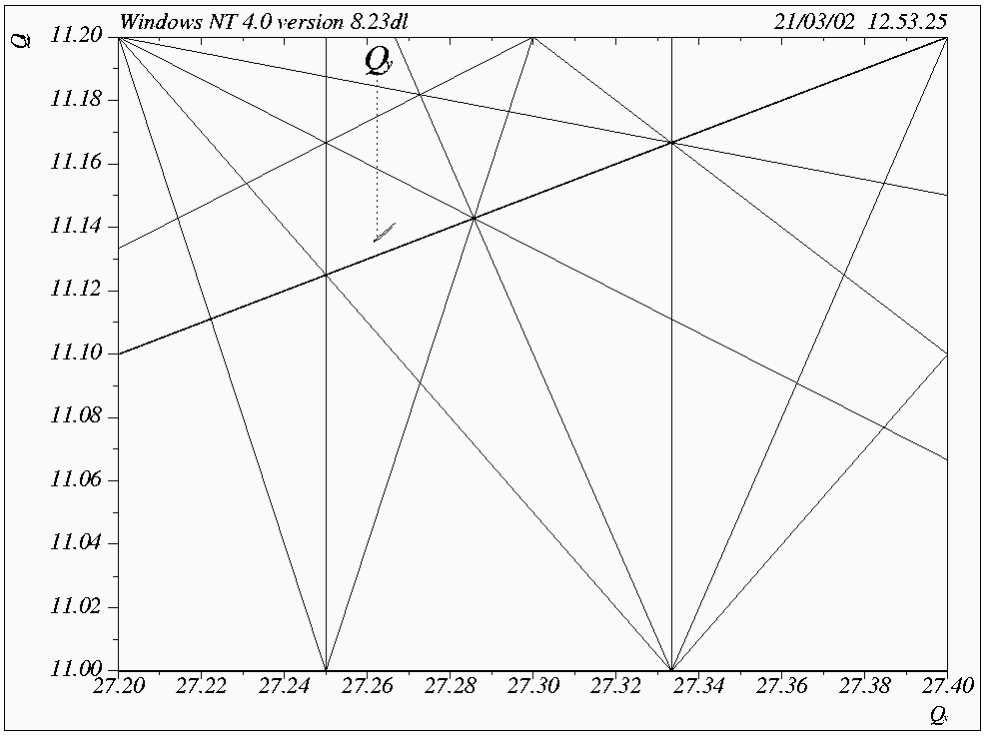

Figure 12

Working point of the MDR lattice. Resonance lines up to fifth order are shown. The tune curve shows variation of the working point with ±2% momentum deviation; space-charge effects are expected to lead to an incoherent vertical tune shift of 0.05.

In principle, the incoherent tune shift is large enough that particles in the beam could cross some higher order resonances (see Figure 12), but it is not immediately clear what effect these resonances would have on the dynamics. We suggest that tracking studies be performed, to investigate further the space-charge effects.

8 Electron Cloud

Electrons generated by a variety of processes may be trapped in the potential well of the beam in a proton or positron storage ring. The dynamical response of the cloud under forces from the beam mediates an interaction between particles in a bunch, or between separate bunches. Under appropriate conditions, the electron cloud can drive instabilities in the beam; instabilities consistent with the expected models have been observed in a number of storage rings[15]. The problem of estimating the impact of the electron cloud instability on a storage ring can be considered in two parts: first, the electron cloud density and distribution must be determined, and second, the behavior and influence of the wake forces resulting from the electron cloud must be found. Both problems are complex, and detailed simulations and analytical models have been developed in attempts to understand the processes involved.

Studies for the NLC MDR are on-going, but we present here some brief comments on the likely impact of the performance of the ring, based on a simple model. The essential features of the model are as follows:

- The number of electrons per unit length in the vacuum chamber is assumed equal to the number of positrons per unit length in the beam (the "neutralization condition").
- During the passage of a single bunch, the electrons are assumed to be concentrated within the bunch, and to oscillate in the field of the bunch. The wake field is then represented by a simple broad-band resonator model.
- Over a longer range, the cloud is assumed to oscillate in a mean beam current, and the wake field is again represented by a broad-band resonator, though with different parameters than for the single bunch case.

The broad-band resonator model has been used for the single bunch by Ohmi et al[16] and by Heifets[17]; and the resonator model for the coupled-bunch case has been considered by Heifets[18]. We note that the real dynamics of the beam and the cloud are significantly more complex than suggested by this model.

Our analysis considers only field-free regions of the lattice. The presence of even weak magnetic fields can make a considerable difference to the complicated dynamics of the electron cloud, and use of solenoid windings around the beam pipe has been found to be an effective method of limiting the effects of the electron cloud.

8.1 Single bunch instability

The beam and cloud are assumed to have transverse gaussian distributions with the same rms sizes. Consideration of the forces acting between particles in the cloud and particles in the bunch leads to the expression for the transverse wake function[16]:

$$W_1(z) = \frac{cR_s}{Q}\sin\left(\frac{\omega_c}{c}z\right) \tag{5}$$

where

$$\frac{cR_s}{Q} = \frac{\gamma\omega_b^2\omega_c C}{\lambda_b r_e c^3} \tag{6}$$

ω_b and ω_c are, respectively, the oscillation frequency of positrons in the field of the electron cloud, and the oscillation frequency of electrons in the field of the bunch:

$$\omega_b^2 = \frac{\lambda_c r_e c^2}{\gamma(\sigma_x + \sigma_y)\sigma_y} \qquad \omega_c^2 = \frac{\lambda_b r_e c^2}{(\sigma_x + \sigma_y)\sigma_y} \tag{7}$$

λ_b and λ_c are the line density of particles in the bunch and in the cloud. Equation (5) does not include any damping of the wake. Since the cloud is a dynamical system responding to a nonlinear force, the oscillations will rapidly decohere. The quality factor Q may be estimated analytically[17] or fitted from simulation. One generally finds that Q is of order 5, but the results of the single bunch instability estimate are insensitive to the exact value.

Including damping of the electron cloud oscillations, the wake function takes the form:

$$W_1(z) = \frac{cR_s}{Q} \mathrm{e}^{-\frac{\omega_c z}{2Qc}} \sin\left(\frac{\omega_c}{c} z\right)$$

and the corresponding wake potential has the usual form:

$$Z_1(\omega) = \frac{c}{\omega} \frac{R_s}{1 + \mathrm{i}Q\left(\frac{\omega_c}{\omega} - \frac{\omega}{\omega_c}\right)}$$

The effect of such an impedance on a bunch may be approached in a number of different ways, of which three are:

1. One solves the linearized Vlasov equation for a given longitudinal phase-space distribution, calculating the frequencies of different synchrotron sidebands to the betatron frequency, and neglecting coupling between the synchrotron modes. Instability may be assumed to occur when the frequency shifts are of the order of the synchrotron frequency.
2. The linearized Vlasov equation is again solved, but mode coupling is included. The growth rates of unstable modes are calculated directly. Only very simple (and rather unrealistic) phase space distributions may be treated by this method.
3. If the resonator period is short compared to the bunch length it may be more appropriate to consider an unbunched or coasting-beam model. An analogous case is the situation where the growth rate of the instability is large compared to the synchrotron frequency, where the standard head-tail theory does not apply. A "post head-tail" theory has been developed to deal with this situation.

It is not entirely clear that any of the above approaches is entirely appropriate to the electron cloud instability, and we do not expect to determine accurately thresholds or growth rates. We may hope, however, to develop some idea of where the proposed parameters of the damping rings lie in relation to the instability regime.

The first approach given above is the simplest[19]. We define an effective impedance for the *l*-th mode:

$$Z_1^{eff}(l) = \frac{\sum_{p=-\infty}^{\infty} Z_1(\omega_{p,l}) h_l(\omega_{p,l} - \omega_\xi)}{\sum_{p=-\infty}^{\infty} h_l(\omega_{p,l} - \omega_\xi)}$$

$$\omega_{p,l} = p\omega_0 + \omega_\beta + l\omega_s$$

where ω_0, ω_β, ω_s are the revolution, betatron and synchrotron frequencies respectively, and

$$\omega_\xi = \frac{\omega_\beta \xi}{\alpha}$$

where ξ is the chromaticity. For a gaussian beam:

$$h_l(\omega) = \left(\frac{\omega\sigma}{c}\right)^{2l} \mathrm{e}^{-\frac{\omega^2\sigma_z^2}{c^2}}$$

The tune of the *l*-th mode is then given by:

$$\frac{\Omega_l - \omega_\beta}{\omega_s} \approx l - \frac{1}{4\pi} \frac{\Gamma\left(l + \frac{1}{2}\right)}{2^l l!} \frac{N_b r_e c^2}{\gamma T_0 \omega_\beta \omega_s \sigma_z} \mathrm{i} Z_1^{eff}(l)$$

Using the NLC MDR parameters, assuming the cloud density given by the neutralization condition and zero chromaticity, we find that $\mathrm{i}Z_1^{eff}(l=0) \approx 1.3$ MΩ/m, and the tune shift for the $l = 0$ mode is approximately –1.8; this suggests that the operating parameters are well above the instability threshold.

Taking the second approach suggested above, we solve the linearized Vlasov equation for a bunch with gaussian distribution in transverse and longitudinal phase space, again looking for the frequencies of the synchrotron sidebands to the transverse dipole mode, but now including the possibility of mode coupling[20]. In this, we follow the procedure of Ohmi et al[16]. Since mode coupling is allowed, the frequencies we find may be complex; the occurrence of complex frequencies indicates the onset of the strong head-tail instability. We retain only the lowest radial mode in the longitudinal phase space, and the tunes of the different modes are then given by the eigenvalues of the matrix $\mathbf{M}$, which has components:

$$M_{ll'} = l\delta_{ll'} - \mathrm{i} \frac{N_b r_e c^2}{4\pi\gamma C \omega_\beta \omega_s} \frac{\mathrm{i}^{l-l'}}{\sqrt{ll'}} \int_{-\infty}^{\infty} \mathrm{d}\omega Z_1(\omega) \left(\frac{(\omega - \omega_\xi)\sigma_z}{\sqrt{2}c}\right)^{l+l'} \exp\left(-\frac{(\omega - \omega_\xi)^2 \sigma_z^2}{c^2}\right)$$

Given the lattice parameters, and bunch charge and dimensions, it is now possible to find the eigenvalues of $\mathbf{M}$.

Table 3

Quantities describing the short-range electron cloud wake.

Quantity	Symbol	Value
Electron cloud density	n_0	2.2×10^{13} m^{-3}
Electron frequency	ω_c	1.0×10^{12} s^{-1}
Positron frequency	ω_b	2.8×10^{6} s^{-1}
Wake function amplitude	cR_s/Q	1.5×10^{8} m^{-2}
Quality factor	Q	5

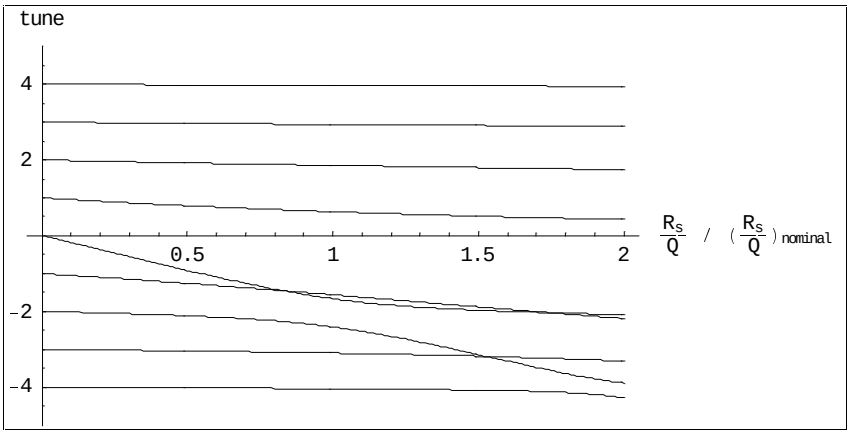

Figure 13

Synchrotron sideband tune as a function of the electron cloud wake function amplitude.

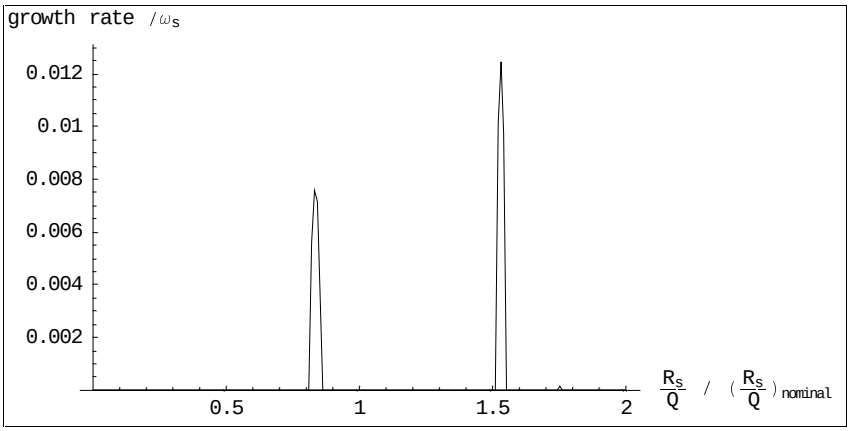

Figure 14

Growth rates of the strong head-tail modes associated with mode coupling. The shortest growth time is 3.6 ms.

The values of the significant quantities are shown in Table 3. We have again used the electron cloud density given by the neutralization condition with the standard beam-pipe radius of 0.016 m. (In the wiggler section the density may be higher because of the narrower pipe of 0.008 m radius, but in the wiggler the magnetic fields could play a significant role.) We plot the solution for the first four synchrotron sidebands as a

function of R_s/Q in Figure 13. Note that to produce the plot, we vary the amplitude of the wake function, while leaving all other parameters unchanged; in other words, the nominal impedance is given by (6), but we investigate what happens if the impedance is larger or smaller than expected. Instability is associated with the tunes of two sidebands merging, which happens on either side of the nominal impedance in the case under consideration. The associated growth rates are shown in Figure 14.

We note that the tune shift of the zero mode is consistent with that found in our first approach to the problem, where we neglected mode coupling. The somewhat unusual behavior of the modes, in that there are very narrow ranges of the impedance where the instability occurs, is a consequence of the fact that the cloud frequency ω_c is larger than the characteristic bunch frequency c/σ_z by a factor of 12. We therefore turn to the third approach to estimating the instability threshold, based on the coasting beam model. In this model, the threshold for the instability is given by[21]:

$$N_{th} = 4\sqrt{\frac{3}{2}}\frac{\gamma C\alpha\sigma_\delta\sigma_z\left|\omega_q-\omega_\xi\right|}{r_e c^2\beta_y\left|Z_1^{eff}(0)\right|}$$

Here, ω_q is the value of ω_ξ at which the real part of $Z_1^{eff}(0)$ takes its maximum value, and $Z_1^{eff}(0)$ is to be evaluated as though the chromaticity were such that $\omega_\xi = \omega_q$. Note that this is not entirely a self-consistent treatment, since we treat the impedance as though it were independent of the bunch charge, which is not the case for the electron cloud. Since we are only interested in whether we are above or below threshold, however, this approach is good enough.

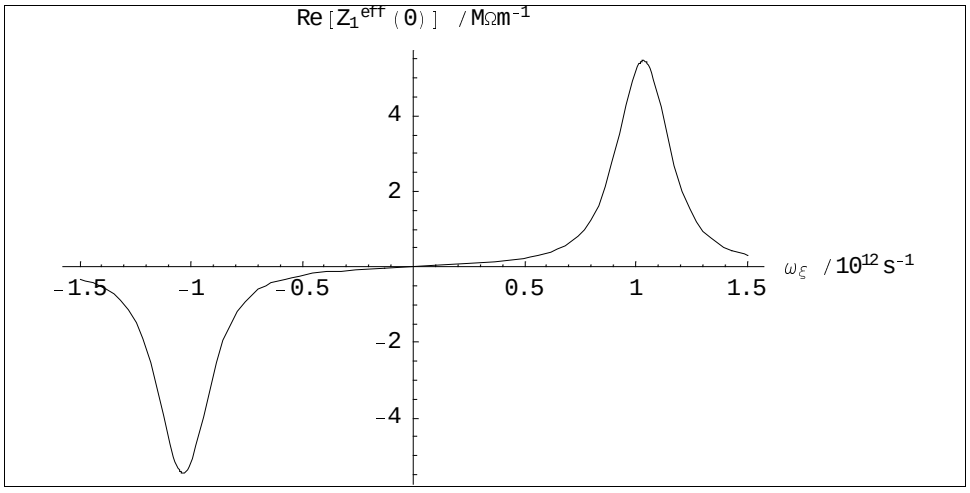

Figure 15

Real part of the zero mode effective impedance as a function of chromaticity.

$\mathrm{Re}\left[Z_1^{eff}(0)\right]$ as a function of ω_ξ is shown in Figure 15; the peak is at $\omega_\xi \approx 10^{12}\,\mathrm{s}^{-1}$, and we find that the threshold bunch charge is just under 10^{10} particles. Thus, all three possible approaches are consistent in indicating that the MDR with the current parameter set is close to, or above, the instability threshold.

The focusing force of the electron cloud also generates an incoherent tune shift[22]. A rough estimate for this tune shift is given by:

$$\Delta\nu_y = K_b \frac{\omega_b^2}{\omega_0^2 \nu_y} \tag{8}$$

where K_b is a cloud bunching factor, allowing for an increased density of the cloud in the positron bunch, beyond that given by distributing the cloud with the same rms widths as the positron bunch. Simulations suggested that this factor could be as much as 15, which would give an incoherent tune shift about 0.3. This is a significant amount, and is likely to have a detrimental effect on the dynamics, though it is difficult to quantify the effect without further work.

8.2 Coupled bunch instability

After a bunch passage, electrons close to the bunch are left with sufficient energy that they reach the wall of the vacuum chamber before the arrival of the next bunch. Electrons further away are kicked by the bunch, but do not perform a complete oscillation, and do not reach the wall before the arrival of the next bunch. Electrons in this region may be thought of as oscillating in the mean field of the beam; this is likely to be a reasonable model, if the period of such oscillations is large compared to the time between bunches.

The potential well of the averaged beam is logarithmic at distances that are large compared to the beam size. We must therefore consider the equation of motion

$$\ddot{y} = -\frac{k^2}{y} \tag{9}$$

where y is the transverse displacement of an electron with respect to the beam orbit. With the initial conditions $y(0) = a$, $\dot{y}(0) = 0$, this has the solution:

$$\sqrt{\ln\left(\frac{a}{y}\right)} = \mathrm{Erf}^{-1}\left(\sqrt{\frac{2}{\pi}}\frac{k}{a}t\right)$$

It is then easy to solve for $y(\pi/2\omega) = 0$, where ω is the frequency of oscillation. We find:

$$\omega = \sqrt{\frac{\pi}{2}}\frac{k}{a} \tag{10}$$

Note that the frequency of oscillation is inversely proportional to the amplitude. This means that coherent oscillations of electrons in the cloud will rapidly decohere, because of the frequency spread.

We assume that the wake field resulting from oscillations of the electron cloud can be modeled as a broad-band resonator, with critical frequency given by (10). From (9), we clearly have $k^2 = 2N_b r_e c^2 / s_b$, where s_b is the bunch separation. To find an appropriate value for the oscillation amplitude, we consider those electrons at distance $r_{\min}$ from the beam, that receive sufficient energy from one bunch passage to kick them to the wall:

$$r_{\min} = \frac{2N_b r_e s_b}{b}$$

where b is the vacuum chamber radius. We simply take $a = r_{\min}$, to write[23]:

$$\omega_c = \frac{bc}{2}\sqrt{\frac{\pi}{N_b r_e s_b^3}} \tag{11}$$

Decoherence of the oscillations leads to a damping of the wake field characterized by a quality factor $Q \approx 5$. A bunch with some transverse displacement initiates coherent oscillations of particles in the cloud. This suggests an amplitude for the wake field:

$$\frac{cR_s}{Q} = \frac{n_0 s_b}{N_b}\frac{\omega_c}{c}L$$

and the wake field is then given by:

$$W_1(z) = -\frac{cR_s}{Q}\mathrm{e}^{-\frac{\omega_c z}{2Qc}}\sin\left(\frac{\omega_c}{c}z\right)$$

For M evenly spaced bunches the frequencies Ω_μ of the different modes are given by[20]:

$$\Omega_\mu - \omega_\beta = \frac{N_b r_e c}{2\gamma\omega_\beta}\sum_{k=0}^{\infty} W_1(ks_b)\mathrm{e}^{2\pi i k(\mu+\nu_y)/M}$$

The imaginary part of Ω_μ gives the growth rate, and the real part gives the coherent tune shift associated with a particular mode. For the MDR case, we consider a ring filled with 714 bunches; i.e. we neglect the 65 ns gap between bunch trains. This is likely to give a pessimistic value for the growth rates, which are shown in Figure 16. Note that we have assumed a cloud density again given by the neutralization condition. The tune shifts are shown in Figure 17. The shortest growth time of any mode is 20 μs. There is considerable uncertainty in this figure, so although it is possible that it may be within the range of a feedback system, it is also possible that the growth rates could be much larger, and difficult to damp.

9 Fast Beam-Ion Instability

Ions generated by interaction between an electron beam and residual gas molecules in the vacuum chamber can be trapped in the beam, and give rise to instabilities. In certain parameter regimes, a fast instability can be manifest, which is not controlled by gaps in the bunch train for the purpose of clearing the ions. Such an instability has been analyzed by Raubenheimer and Zimmermann[24], and has been observed in a number of machines[25].

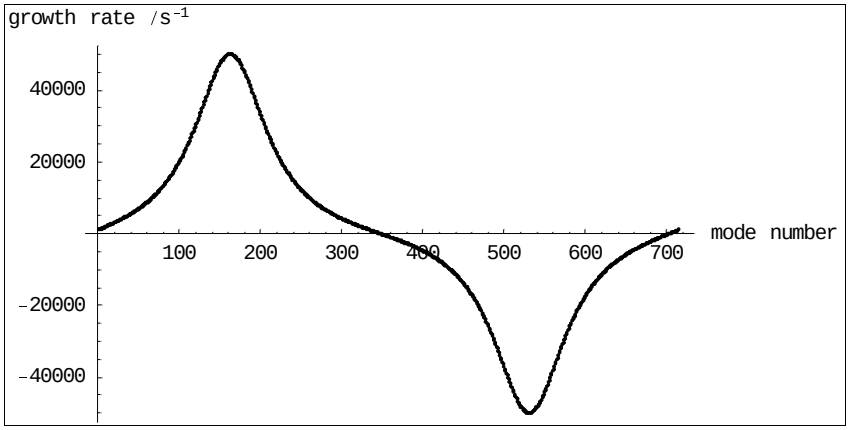

Figure 16

Growth rates of the coupled bunch modes driven by the electron cloud.

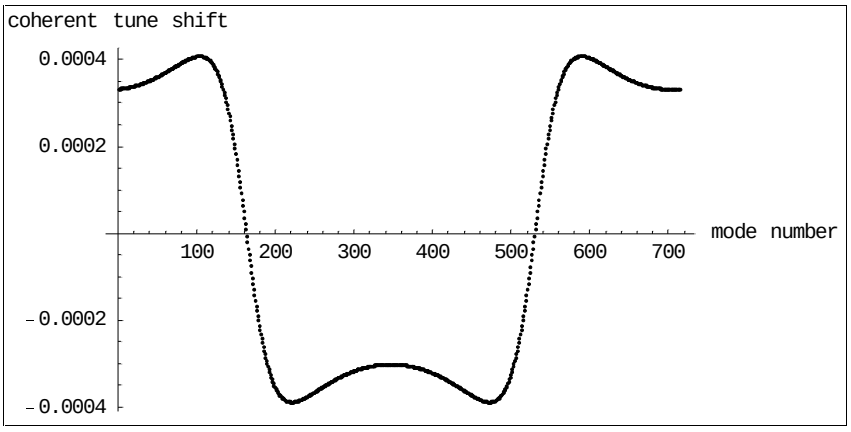

Figure 17

Tune shift of the coupled bunch modes driven by the electron cloud.

In the limit for large times t, the vertical action of the final bunch in a train grows as[26]:

$$J_y \approx \frac{J_{y0}}{8\pi\sqrt{t/\tau}} \exp\left(2\sqrt{\frac{t}{\tau}}\right)$$

where

$$\tau^{-1}\left[\mathrm{s}^{-1}\right] \approx 5\,p[\mathrm{Torr}]\frac{N_b^{3/2} n_b^2 r_e r_p^{1/2} s_b c}{\gamma\sigma_y^{3/2}\left(\sigma_x+\sigma_y\right)^{3/2} A^{1/2}\omega_\beta}$$

p is the residual gas pressure, n_b the number of bunches in the train, r_p the classical radius of the proton, and A is the atomic mass number of the residual gas molecules leading to the instability. We have assumed an ionization cross-section of 2 Mb. If the oscillations grow from Schottky noise, then the initial vertical action may be estimated as:

$$J_{y0} \approx \frac{\sigma_y^2}{2N_b n_b \beta_y} \tag{12}$$

The growth times predicted from this theory for the NLC are shown as a function of pressure in Figure 18; we have assumed the residual gas is CO, for which $A = 28$. At a pressure of 1 nTorr, the growth time is 160 ns, which is certainly too fast for a feedback system to damp. We note that if the initial betatron amplitude is given by equation (12), then about 300 rise times are required before the oscillation amplitudes become comparable to the beam size.

The collected ions also lead to an incoherent tune shift, which may again be estimated from (8) and the first of equations (7), where now we use the ion line density:

$$\lambda_c \left[\mathrm{m}^{-1}\right] \approx 5 p[\mathrm{Torr}] N_b n_b$$

We assume a bunching factor of 1, since the ions are slow to respond to the forces from the beam. For the MDR, we find an incoherent tune shift of 0.005 for a residual pressure of 1 nTorr.

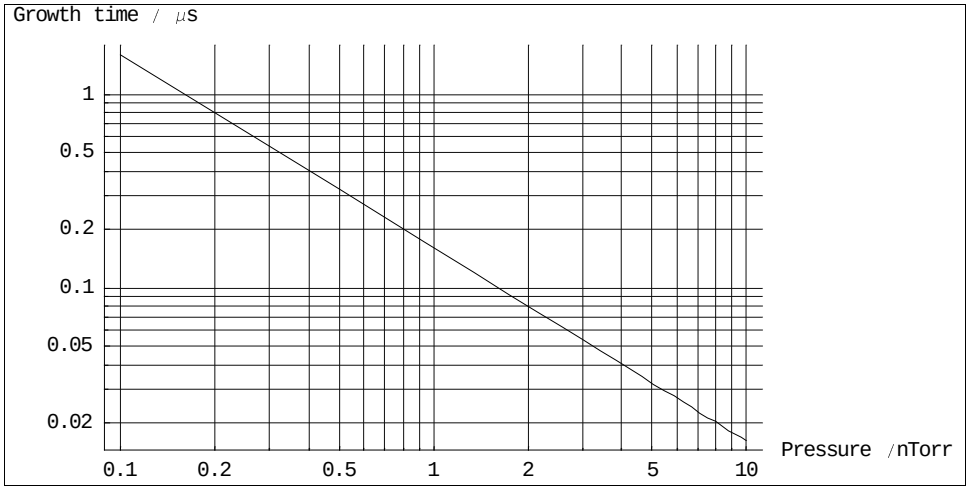

Figure 18

Fast beam-ion instability growth time as a function of pressure.

Although the incoherent tune shift appears not too large, the growth time from the fast beam-ion instability needs to be addressed, and further studies should include detailed tracking simulations. Possible remedies are discussed in Reference 24.

10 Conclusions

- If the low impedance suggested by the current modeling can be achieved, bunch lengthening should be small; the machine should operate some way below the threshold for microwave instability.
- The growth of coupled bunch modes from resistive wall impedance and higher order modes in the cavities, can be controlled by a feedback system.

- The short Touschek lifetime could make commissioning and tuning the machine difficult. It would be desirable to improve the dynamic acceptance of the ring, and to have an RF system specified for more than the current 1.5% momentum acceptance. An increase in bunch length, and a method of coupling the transverse emittances in a controlled manner would also be of benefit.
- Intra-beam scattering is likely to pose a significant restriction on the performance of the damping ring with the current design. There are various ways to minimize the effects of IBS, but also considerable uncertainty in the theory. We propose that experimental studies with the aim of testing the theory be continued, and that different methods for overcoming the limits imposed be carefully considered.
- The phase transients from beam loading in the main RF cavities are unlikely to pose any significant problems. There is a different situation regarding higher harmonic cavities, which might otherwise be used for reducing IBS effects by lengthening the bunch. It seems unlikely at present that higher harmonic cavities could be used as a solution to IBS.
- The space-charge tune shift is approaching the regime where it could limit the dynamical stability of the beam. Further work is needed, including detailed simulations (and possibly, experimental studies), before it can be stated with confidence that space-charge effects will not be a problem.
- Theoretical studies of single bunch and coupled bunch instabilities from electron cloud are continuing. Much has been learned from observations at existing machines, and progress is being made in both analytical studies and in simulations. It appears highly likely that electron cloud instabilities will limit the performance of the positron damping ring, if preventive measures are not taken. It is important to continue experimental and theoretical work, in the direction of predicting the thresholds and growth rates with confidence, in a variety of situations (effects of magnetic fields, vacuum chamber coatings etc.) A large amount of data already collected needs to be fully understood.
- The precise effects on the damping ring performance of the fast beam-ion instability are uncertain. It is likely that a pressure below 1 nTorr will be needed, at least in some parts of the machine, if adverse effects are to be avoided. Further work is needed, and should include simulations and experimental studies.
- We have not so far considered the effects of transients from the injection process. Injected beams with large offsets could have a detrimental effect on stored beams. This is a further important area where more work is needed.

Acknowledgements

We should like to thank Karl Bane, John Byrd, Miguel Furman, Sam Heifets, Mauro Pivi and Tor Raubenheimer for useful comments and discussions.

References

[1] A. Wolski, "Lattice Description for NLC Main Damping Rings at 120 Hz", LCC-0061, April 2001.

[2] S. de Santis, "Coupled Bunch Instabilities in the NLC Damping Rings", LCC-0069, May 2001.

[3] R.D. Kohaupt, "On Multi-Bunch Instabilities for Fractionally Filled Rings", DESY 85-139, 1985.

[4] R.A. Rimmer et al, "RF Cavity R&D at LBNL for the NLC Damping Rings, FY2000/2001", LCC-0072, October 2001.

[5] C. Ng, unpublished presentation, 1999. J. Corlett et al, "Impedance and Instabilities in the NLC Damping Rings", Proceedings PAC 2001.

[6] "Zeroth-Order Design Report for the Next Linear Collider", SLAC Report 474, May 1996.

[7] H. Wiedemann, "Particle Accelerator Physics II", Springer, 1995.

[8] T.O. Raubenheimer, PhD Thesis, SLAC-387, Section 2.3.1, 1991.

[9] J.D. Bjorken and S.K. Mtingwa, "Intrabeam Scattering", Particle Accelerators **13** p.115, 1983.

[10] See for example, K.L.F. Bane et al, "Intrabeam Scattering Analysis of ATF Beam Measurements", SLAC-PUB-8875 (Revised), July 2001.

[11] K. Kubo, "Ratio of Relative Increase of Vertical and Horizontal Emittances Due to Intra-Beam Scattering in ATF DR", ATF Internal Report, ATF-00-15, December 2000.

[12] K. Kubo, "Beam Development in the ATF", Talk given at 7th International Study Group Meeting, March 2001.

[13] J. Corlett et al, "Meaurements of Intra-Beam Scattering at low emittance in the Advanced Light Source", Proceedings HEACC 2001.

[14] J.M. Byrd, S. de Santis et al, "Transient Beam-Loading Effects in Harmonic RF Systems for Light Sources", submitted to PRST-AB, 2002.

[15] See for example, F. Zimmermann, "The Electron Cloud Instability: Summary of Measurements and Understanding", Proceedings PAC 2001, and references therein.

[16] K. Ohmi, F. Zimmermann, E. Perevedentsev, "Study of the Fast Head-Tail Instability Caused by the Electron Cloud", CERN-SL-2001-011 AP, May 2001.

[17] S. Heifets, "Wake Field of the E-Cloud", SLAC-PUB-9025, November 2001.

[18] S. Heifets, "Results of the Qualitative Analysis of the E-Cloud Formation", unpublished, January 2002.

[19] A. Chao, "Physics of Collective Beam Instabilities in High Energy Accelerators" Wiley, 1993, p.346.

[20] A. Chao, "Physics of Collective Beam Instabilities in High Energy Accelerators" Wiley, 1993, the latter part of chapter 6.

[21] P. Kernel, R. Nagaoka, J.-L. Revol and G. Besnier, "High Current Single Bunch Transverse Instabilities at the ESRF: A New Approach", Proceedings EPAC 2000.

[22] M.A. Furman and A.A. Zholents, "Incoherent Effects Driven by the Electron Cloud", Proceedings PAC 1999.

[23] This is larger by a factor $\sqrt{2\pi}$ than the corresponding quantity used by S. Heifets in reference 18.

[24] T.O. Raubenheimer and F. Zimmermann, "Fast Beam-Ion Instability", Phys.Rev.E 52, p.5487, 1995.

[25] See for example J. Byrd et al, "First Observations of a Fast Beam-Ion Instability at the ALS", Proceedings EPAC 1998.

[26] "Zeroth-Order Design Report for the Next Linear Collider", SLAC Report 474, May 1996, page 189.